Tellus (1983), *35B*, 329–345

Mean fields of precipitable water over the Indian Ocean during the 1979 summer monsoon from TIROS-N soundings and FGGE data

By DANIEL L. CADET, *Department of Meteorology, Florida State University, Tallahassee, Florida 32306, U.S.A.*

(Manuscript received March 22; in final form May 30, 1983)

ABSTRACT

An assimilation of precipitable water in three layers (Surface–700 mb, 700–500 mb, 500–300 mb) as inferred by TIROS-N precipitable water data and Level III-b humidity fields from ECMWF (European Center for Medium Range Weather Forecast) during summer 1979 is presented. The domain of the study is the summer MONEX area (30–120° E; 30° N–30° S) and the period covers May, June, July, August and the first half of September 1979. An objective analysis of the satellite data was carried out every 12 hours at 0000 and 1200 GMT. To overcome the lack of satellite data over cloudy areas, some subjective data were inserted taking mean TIROS-N temperature profiles in disturbed areas and assuming a certain profile of relative humidity. The fields obtained from the assimilation of TIROS-N data were merged with Level III-b fields. During the merging process higher weight was given over land to Level III-b fields than to TIROS-N fields whereas the opposite prevailed over the ocean. The accuracy of the final fields has been estimated using the dropsonde soundings performed from research aircraft during MONEX-79. The relative accuracy is about 13%.

The fields reveal the variations of precipitable water associated with the establishment of the SW monsoon. Preonset conditions were characterized by dry air over the Arabian Sea and humid air over the equator. Two weeks prior to the onset, maxima of PW began to move from equatorial regions northward to the Arabian Sea. Post-onset fields show the existence of dry air along the African coast and western Arabian Sea due to the inversion layer, and humid air over the eastern Arabian Sea where the inversion layer weakens and convection develops. The major break which occurred around mid-July affected the fields of precipitable water. The first week of the break in the activity of the monsoon was characterized by a drop of about 15% of the amount of precipitable water over the Arabian Sea compared to an active period. The fields of vertical wind reveal that convection was inhibited over the eastern Arabian Sea during the break. Two-latitude cross-sections of weekly mean fields were constructed at different longitudes. They show the time evolution of the fields associated with the onset of the Southwest monsoon and with its active/break cycle.

1. Introduction

The southwest monsoon which takes place during the summer months affects the countries of the Indian subcontinent. It is characterized by a flow of moist air northward across the equator and into southern Asia as shown by different studies (Saha, 1970; Saha and Bavadekar, 1973; Cadet and Reverdin, 1981b). These studies as well as others (Ramage et al., 1972; Cadet and Reverdin, 1981a) have also pointed out the role of the southern tropical Indian Ocean besides the Arabian Sea as an important moisture source for the Asian summer monsoon. Monthly mean fields of total precipitable water vapor over India were determined by Ananthakrishnan et al. (1965). The fields point out the large increase of the moisture content of the atmosphere associated with the onset of the monsoons.

These studies were mainly based on the analysis of surface and radiosonde data available at a few stations located over and around the Indian Ocean. Most of the papers were dealing with monthly mean water vapor balance over the Indian Ocean to determine the importance of cross-equatorial flux compared to evaporation over the Arabian Sea for supplying the Indian subcontinent with moisture. Cadet and Reverdin (loc. cit.) studied the fluctuations of the water vapor flux at the surface level across different sections in the Indian Ocean. They found that the flux was fluctuating with a period around 10 days corresponding to one of the natural oscillations of the large-scale monsoon system. The monsoon is also characterized by a break and active cycle with a period in the range 30–50 days. Cadet (1983) has shown that this cycle can affect the circulation over the Arabian Sea and consequently the transport of water vapor.

One of the objectives of the satellites of the TIROS-N series is to infer operationally water vapor profiles from the measurements of the outgoing radiations reaching the High Resolution Infrared Sounder (HIRS) onboard the satellites, within specified spectral bands. One of the advantages of the satellite technique is its global coverage, at least twice a day during very long periods of time. The scope of this paper is to analyze precipitable water (called PW thereafter) over the Indian Ocean inferred by the TIROS-N satellites and from Level III-b humidity data determined by ECMWF during summer 1979. The TIROS-N data, provided by NOAA, concerns precipitable water in three layers: surface–700 mb, 700–500 mb and 500–300 mb. The Level III-b data give the relative humidity and temperature at different pressure levels (1000–850–700–500–400 and 300 mb).

This work presents the May, June, July, August and half-September analysis. The domain extends from 30° to 120° E longitude and from 30° S to 30° N latitude. PW in the three layers were determined every 12 hours from 1 May to 15 September 1979 on a 2° latitude by 2° longitude grid system by objective analysis techniques. Due to the inability of TIROS-N to derive humidity information in cloudy areas, some subjectively analyzed data were added in disturbed regions. The analyzed fields were merged with Level III-b data to obtain the final fields. In this first part, the mean fields and their evolution are presented and discussed. Fluctuations of the precipitable water fields in relationship with the different periodicities of the summer monsoon will be discussed in a companion paper. Results on water transport over the Indian Ocean using TIROS-N moisture fields and Level III-b humidity and wind fields will be presented later.

2. The original data and the preparation of final products

2.1. *TIROS-N data*

The data used in the present analysis were provided by the TIROS-N/NOAA satellites which are of the latest generation of operational sun-synchronous orbiting satellites. The complement of infrared and microwave instruments aboard a satellite provides with a complete global coverage of vertical temperature and moisture profiles data every 12 hours (after the end of the first half of 1979 the launching of a second satellite reduced the time interval to 6 hours). A description of the TIROS-N Operational Vertical Sounder (TOVS) has been given by Smith et al. (1979). The TOVS instrumentation includes three channels directed to the retrieval of precipitable water. They are positioned spectrally at 8.3, 7.3 and 6.7 m and roughly sense the troposphere from the surface to 300 mb. Soundings are derived by utilizing methods established by Smith and Woolf (1976). It is a statistical approach that uses eigenvectors of covariance matrices to retrieve soundings. The coefficients used to derive soundings from radiance observations are generated by a set of collocated cloud free radiances and radiosonde observations. The coefficients are updated weekly and the previous week's coefficients are used in the retrievals. One set of coefficients is generated for the latitude zone 30° N–30° S. For moisture retrievals, two possible paths exist. They correspond to a completely clear spot or a partly clear area. In this latter case, a technique is used to check adjacent field of view to filter the effects of clouds and derive a clear sounding. As a practical matter the moisture retrievals occur mainly in clear air with a deficiency over disturbed areas (Gruber and Watkins, 1979). These authors also noted by comparing moisture profiles from TIROS-N soundings and from radiosoundings that while the retrievals are deficient in depicting the vertical structure, they can depict moisture content in certain layers of the atmosphere without an important bias. However, they noted that TIROS-N sounding is underestimating PW in a deep moist layer whereas there is an overestimation for a relatively dry layer. This is related to the inability of the regression solution to depict extreme conditions. In other words an abnormal situation occurring somewhere is not going to be properly represented because the regression coefficients of the last week do not contain the information.

2.2. *Objective analysis*

NOAA provided with data giving the PW in three layers: surface–700 mb, 700–500 mb and 500–300 mb. Due to problems explained above, instead of deriving humidity values at different pressure levels from the original data, we directly analyzed the PW data. The objective analysis was accomplished by use of the method of successive corrections (Bergthorsson and Döös, 1955; Cressman, 1959) adapted by Tripoli and Krishnamurti (1975) to the analysis of low-level flow over the GATE area. The scheme involves the successive modifications of an initial guess field on the basis of observed data. The assimilation is quite similar to that one developed by Tripoli and Krishnamurti (1975) where a detailed description may be found. In carrying out the analysis, a total of four correcting passes through the field was made with the radius of influence decreasing with each scan (5°, 4°, 3°, 2°). The last radius of influence was given a small value due to the even distribution of the data. Bad data were rejected according to criteria varying with each scan. In the successive correction method, the difference between the observation and the value of the guess field is determined at the location of the observation. When this difference exceeds a rejection criterium, the observation is rejected. For the four scans, the rejection criteria were 20, 15, 10 and 5 for the first layer; 8, 5, 3 and 2 for the second layer; and, 4, 3, 2 and 1.5 for the last layer. The determination of these rejection criteria is rather subjective. To reach the final values, different sets of values were tested. For each set the objectively analyzed fields were screened against initial values as well as the number and the values of rejected observations. The grid was taken to be a 2° latitude by 2° longitude mesh from 30° E to 120° E and from 30° S to 30° N.

The objective analysis scheme is based on the modification of a first-guess field with existing data. As the density of data is fairly good over all the domain (Fig. 1), the choice of a first guess field is

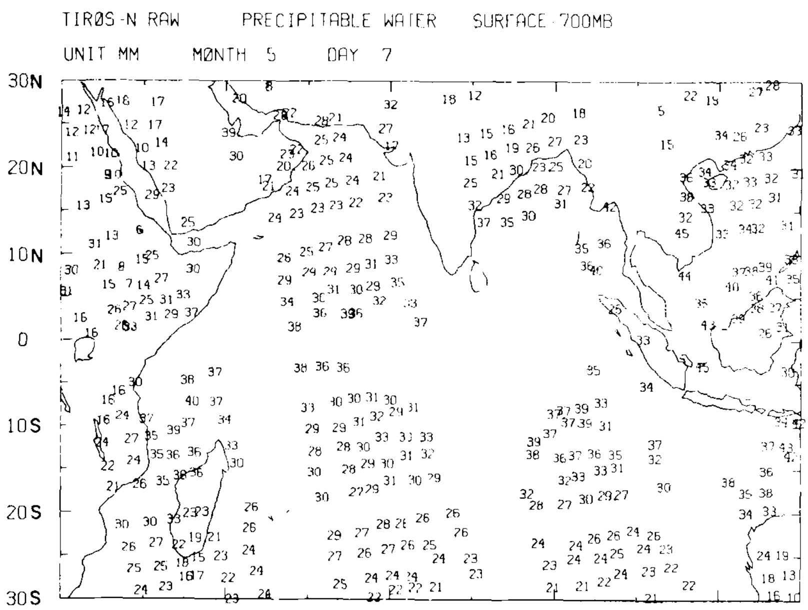

Fig. 1. TIROS-N soundings obtained around 1030 GMT over the Indian Ocean on 7 May 1979. Precipitable water within the layer surface–700 mb.

less important than in the case of other data which may be scarce over certain areas. Because of the relatively slow evolution of the moisture parameter, the previous field was used as a first guess field. This also insures temporal continuity in the analyzed fields. In order to obtain a reliable field on 1 May, we started the objective analysis on 29 April using as a first guess field constant moisture fields of 30 mm for the first layer, 10 mm for the second layer and 2.5 mm for the last layer.

One of the problems about the use of satellite information is their asynoptic character. This kind of data is not well distributed about the hour of the assimilation: the sampling along a latitude circle is made at the same local time. For example, the eastern part of the Indian Ocean was covered during one satellite pass around 2030 GMT and during another pass around 09 h 30 GMT. The section of the ocean located westward of the first strip was covered around 0000 GMT and 12 h 30 GMT and i.e., even for adjacent regions the data are gathered at different hours of the day. This sampling can have an effect on the estimation of wavenumber-frequency spectra (Hayashi, 1980) but for our purpose this sampling effect is negligible because precipitable water in the three layers does not change very much over a couple of hours. In order to have the minimum effects, and to obtain fields at synoptic hours, the objective assimilation of the data has been made twice a day at 0000 and 1200 GMT which corresponds to the two times of the day when the satellite was over the domain. To perform an analysis, data obtained during satellite passes over about 30 hours were assimilated. For example, for an analysis at 1200 GMT the data during the previous night passes, during the day passes and during the following night passes were used. The time weighting function had a gaussian distribution with a weight equal to 0.4 assigned to data 12 h apart from the time of analysis. Similar time weighting functions were used by other authors (Tripoli and Krishnamurti, 1975). It must also be noted that the data corresponding to one pass of the satellite do not overlap with the data obtained during the previous pass or the next pass of the satellite. The closest two edges of the strips covered during two successive passes are separated by about 4–5° and some features may be missed if only data around one time are assimilated. The use of data gathered within ± 15 h from the time of analysis overcomes this problem.

Because the moisture retrievals were obtained in clear or near clear air areas, there is usually a lack of data in the very cloudy regions. These regions are of interest for the description of the moisture fields because they usually correspond to intense cyclonic circulation which may enhance rainfall over certain areas. Thus, on certain days a lack of data may prevail over squares as large as 5° and unrealistic grid point values may result with some underestimation of the water vapour content. In order to reproduce realistic grid point values in very cloudy areas we made a subjective analysis in order to insert some values in the very cloudy areas corresponding to some cyclonic activity. Thompson and West (1967) and Smigielski and Mace (1970) developed a method to estimate atmospheric relative humidity by using satellite cloud photographs. Different categories were defined to classify clouds observed in the satellite pictures. Most of the clouds found over the Indian Ocean are mainly convective clouds north of about 10° S or associated with frontal zones in the Southern part of the domain. According to the previous studies, these categories correspond to an average relative humidity above 80% between the surface and 500 mb.

Satellite imagery during summer 1979 was analyzed to determine the position of the cloudy areas and their extension. A mean temperature profile determined from TIROS-N temperature soundings (the microwave sensors allow the determination of temperature profile even in cloudy areas) was determined over each cloudy area. The quality of TIROS-N and NOAA-6 satellite soundings was discussed by Gruber and Watkins (1982) for clear and cloudy retrievals. During summer 1979 the mean difference between satellite-derived and radiosonde profiles was less than -0.3 K in clear conditions and less than -1 K in cloudy areas. TIROS-N data do not contain the temperature at specific pressure levels but a mean temperature over certain layers. However, it gives the skin temperature of the surface (land and ocean). From this information and assuming a linear variation between the levels, the temperature at the different pressure levels was determined. The profile of relative humidity was assumed to be 90% between the surface and 700 mb, 80% between 700 mb and 400 mb and 70% between 400 and 300 mb, and the PW within the three layers was determined. The assumption of relative humidity profile was tested with some of the dropsonde profiles obtained during MONEX (Bolhofer et al., 1981). Fig. 2 shows a comparison between the mixing ratio profile obtained from the dropsonde launched in a disturbed area and the mixing ratio profile computed with the assumed profile of relative humidity. There is good agreement between the two curves showing that this profile gives reasonable values of precipitable water in disturbed areas. In the assimilation scheme the reliability factor of the bogus PW data was 1/5 of the reliability factor of the TIROS-N data. Different values of this reliability factor were tested. The tuning of this reliability factor to 20% of the reliability factor of TIROS-N data seemed to give the best results. Similar ratios between more and less reliable data were used by other authors (Tripoli and Krishnamurti, 1975).

The influence of the bogus data on the final fields can be evaluated especially during days with important cloudiness over certain regions. Fig. 3 gives the cloud cover on 7 May, i.e. before the onset of the monsoon. Large cloudiness can be noted over the equator from about 60° E to 100° E and

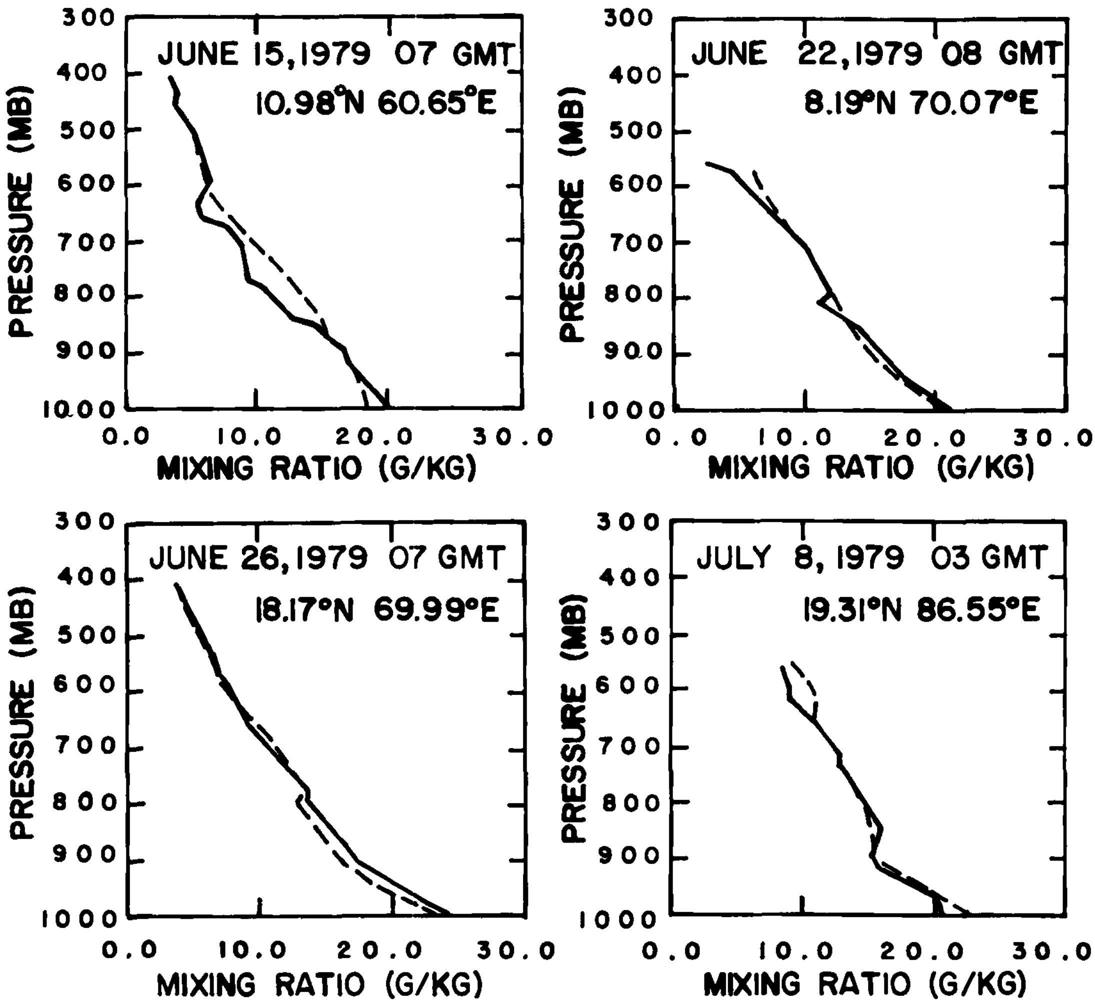

Fig. 2. Humidity profiles from dropsondes over the Arabian Sea. The solid line gives the actual profile and the dashed line gives the profile determined with the assumption of a relative humidity of 90% between the surface to 700 mb, 80% between 700 and 400 mb and 70% above.

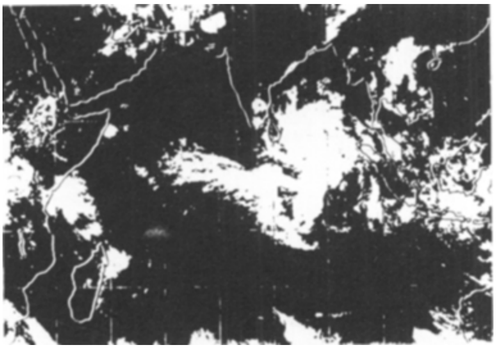

Fig. 3. Cloud cover over the Indian Ocean on 7 May, 1979 from Defense Meteorological Program satellite.

over the area of formation of a cyclone around 85° E and 5° N. Another cloudy area extends from North Madagascar to the east coast of Africa near the equator. These zones also appear on the map of the raw TIROS-N data (Fig. 1): no PW information was retrieved over the disturbed areas. Fig. 4 gives the analyzed PW field for the first layer based only on TIROS-N data. The cloudy areas appear as zones where the humidity is slightly higher than over the other parts of the Indian Ocean. However, no details appear. On the analyzed field based on TIROS-N data and bogus data (Fig. 5) humidity in the cloudy areas is largely enhanced. More details also appear and the position of the convective cloud clusters can be clearly noted.

2.3. *Merging with Level III-b fields*

Level III-b data were produced at the European Center for Medium Range Weather Forecast (ECMWF) using an assimilation scheme described by Bengtsson et al. (1982). The data sets consist of the wind (three components), the temperature, the geopotential height and the relative humidity at different pressure levels and the pressure at the mean sea level. The levels relevant to our analysis are the 1000, 850, 700, 500, 400 and 300 mb levels. This set of analyzed and dynamically derived fields were obtained from the original FGGE data collected within a 3-month cut-off. The data assimilation used a multivariable optimum interpolation analysis, a non-linear normal mode interpolation and a high-resolution forecast that produces a first estimate for the subsequent analysis. The analysis consists of two parts, one for a simultaneous analysis of surface pressure, geopotential and wind and another for humidity. Optimum interpolation is used for the first set of parameters whereas at each layer, water content is derived with a correction method. High-speed gravity waves have been eliminated with a non-linear normal mode initialization. Finally a semi-implicit gridpoint model generates the first-guess prediction fields.

Level III-b data for the domain of the study were stripped out from the global data sets for the period covering our study (1 May–15 September). As the mesh size of the Level III-b fields is 1.875°, a two-dimensional cubic-spline interpolation was used to obtain these data on a 2° mesh corresponding to the analysis of the TIROS-N precipitable water. To compute precipitable water in the three different layers, the geopotential height data and the elevation of the surface were used to determine the values of relative humidity and temperature, as

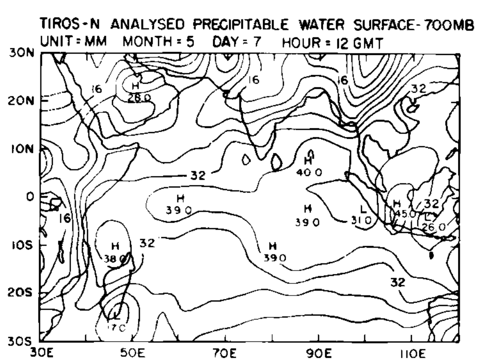

Fig. 4. Analyzed field of precipitable water for the layer surface–700 mb on 7 May from assimilated TIROS-N data.

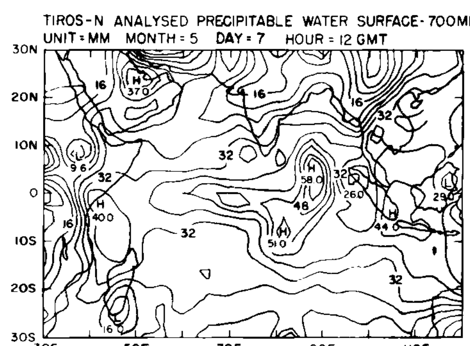

Fig. 5. Same as Fig. 4 except bogus data have been used in cloudy areas.

well as the pressure, at the surface level. The trapezoidal rule was applied to compute precipitable water from the values of mixing ratio at different levels. Values determined in the first layer give the precipitable water existing between the surface and 700 mb. Thus over the Himalayans precipitable water in the first layer is equal to zero because the surface lies at a higher height than the 700 mb pressure level. Synoptic hours for Level III-b data are 00 and 12 GMT except during the special observing period (5 May to 5 July) when analyses were performed every 6 hours. As TIROS-N precipitable water fields were derived every 12 hours, only Level III-b fields at 00 and 12 GMT were used.

During the merging process, different weights were given to the TIROS-N and Level III-b fields. Level III-b humidity fields at the different pressure levels and during all the period were plotted. During certain periods (mainly in May), some parts of the Indian ocean, e.g. north Arabian Sea, eastern equatorial and south-west Indian Ocean depicted unrealistic low values of relative humidity at all levels. However over land, the accuracy of Level III-b fields appears good, because a larger number of observations was available to derive the fields, than over ocean. Because of the problems found over the ocean on Level III-b fields, it was assumed that over the ocean, TIROS-N derived fields are more accurate than Level III-b fields. Fig. 6 gives the weights given to the two data sets during the merging process as a function of the relative difference. Over the ocean the relative weights of TIROS-N and FGGE data depend on their relative difference. When this relative difference increases, the weight given to the TIROS-N data increases whereas the weight given to the FGGE data decreases. Over land, FGGE data being assumed to be a better data set than TIROS-N derived fields, the opposite prevails. To obtain the final relative weights between TIROS-N and FGGE data, different sets were tested. To insure continuity at the land–ocean boundary, the merging at each grid point was made over 9 points. The weight at the points located at 2 degrees from the central point were given a weight equal to half the weight of the central point.

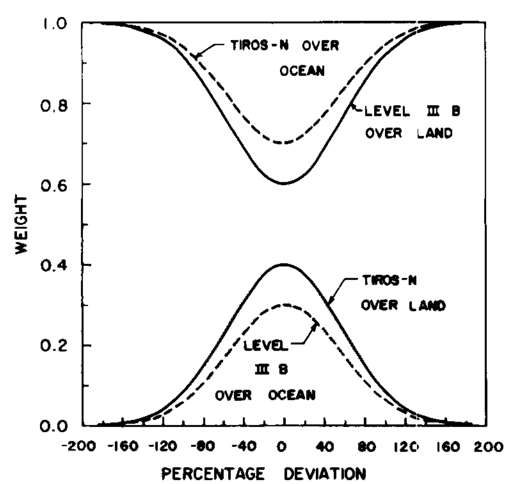

Fig. 6. Relative weights given to the TIROS-N/bogus data derived fields and to the FGGE level III-b fields during the merging process.

Fig. 7 gives the final field of PW on 7 May 1979 at 12 GMT for the layer surface 700 mb. This field reflects well the cloud structure as seen on Fig. 3. The high values depicted on Fig. 5 at the center of the cloud clusters have been reduced during the merging process.

2.4. *Accuracy of final fields*

This accuracy has been estimated using the dropsonde data obtained from aircraft during the MONEX experiment (Bolhofer et al., 1981). These downward soundings have been made in three regions: over the Arabian Peninsula, the Arabian Sea and the Bay of Bengal. The precipitable water in the three layers from the dropsondes was compared to our fields of PW. This comparison was made as follows. The values of precipitable

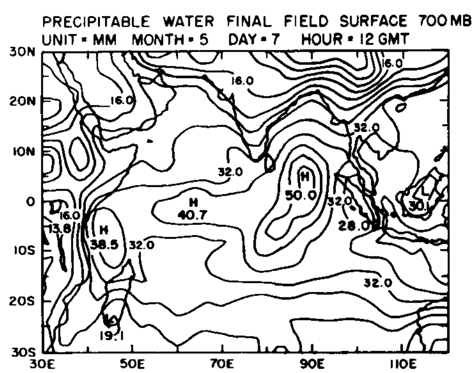

Fig. 7. Final field on 7 May resulting from the merging of TIROS-N/bogus data derived fields and of FGGE level III-b fields.

water at nine grid points around the position of the dropsonde profile were linearly interpolated in time from the assimilated fields at 00 and 12 GMT. Then from these values, the parameter at the location of the dropsonde profile was determined using a nine-point Lagrangian interpolation formula. Fig. 8 gives the result of this comparison. The number of comparisons is given at the upper left side of the graph. This gives a relative difference of about 13%. The line of best fit shows that in each of the two lowest layers, a regression line can be determined. These regression lines have been determined. They are slightly tilted indicating that the amount of PW in very humid areas could be slightly underestimated. The amount of PW from dropsonde may also be overestimated. Gupta (1981) made a comparison between dewpoint temperatures obtained from dropsondes and from the MONEX ships. The results of that study indicate that dewpoint temperatures from the downward soundings are higher than that from upward soundings. This suggests the dropsonde humidity data might have been overestimated. The underestimation of final fields of PW can also arise because satellite-derived temperature profiles were used to compute PW values in disturbed areas. The negative bias found between satellite-derived and radiosonde temperature profiles (Gruber and Watkins, 1982) can give an underestimation of PW of a few percent. Because the use of the regression lines to change the final fields would affect them by only

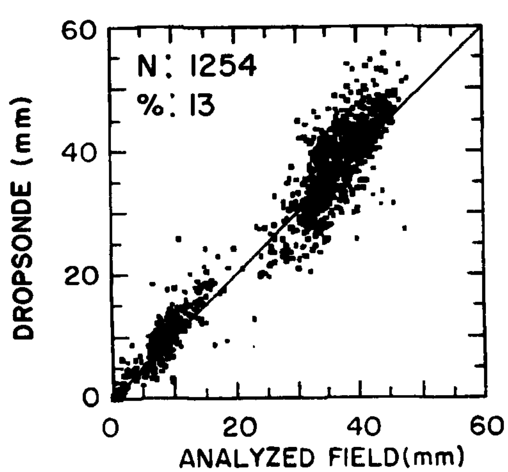

Fig. 8. Scatter plots of the dropsonde precipitable water against the analyzed field of precipitable water.

a few percent and some uncertainties, the final fields were not modified.

It must be noted that Pathak (1982) compared the TIROS-N water vapor data with dropsonde (aircraft) and upsonde (ships) soundings during May–July 1979 over the Indian Ocean. Whereas this last comparison does not include any soundings in disturbed areas, the RMS is around 10%, very near our result.

Monthly, biweekly and weekly fields are shown in the next two sections. The variations of the fields are within the analysis error. However, these fields can be considered as meaningful. Mean fields over a certain period are computed and consequently the error is less than 10–15%. Furthermore, as we are interested in following the evolution of the fields, the relative accuracy which is less than 10–15% must be considered.

3. Mean fields

To determine the evolution of precipitable water during the summer 1979, the monthly mean fields in the three different layers have been computed for May, June, July and August.

Fig. 9 gives the mean fields in the first layer between the surface and 700 mb. In May (Fig. 9a) the largest amount of PW is found over the equator from the Arabian coast up to the Pacific Ocean with a northward tilt as one goes eastward. During the pre-onset conditions, the 32 mm contour line does not extend north of 7° N. In June (Fig. 9b) during which the onset of the monsoon took place (the date of the onset was around 17 June), an increase of PW can be noted at the equator east of 60° E and also over the Arabian Sea and over the Bay of Bengal. The 32 mm contour line now follows the coastal lines north of 10° S. This indicates an intrusion of moist air over the Arabian Sea from the southern hemisphere and also an increase of evaporation due to the build up of the circulation during the onset of the monsoon. The large values of PW over the Arabian Sea also result in the northward progression of the zone of convective activity during the onset phase. In July (Fig. 9c) the highest values of PW are found east of 65° E in the northern part of the Arabian Sea and over the Bay of Bengal. It can also be noted that the 32 mm contour line runs along 55° E north of 10° S. The air mass within 10 degrees off the

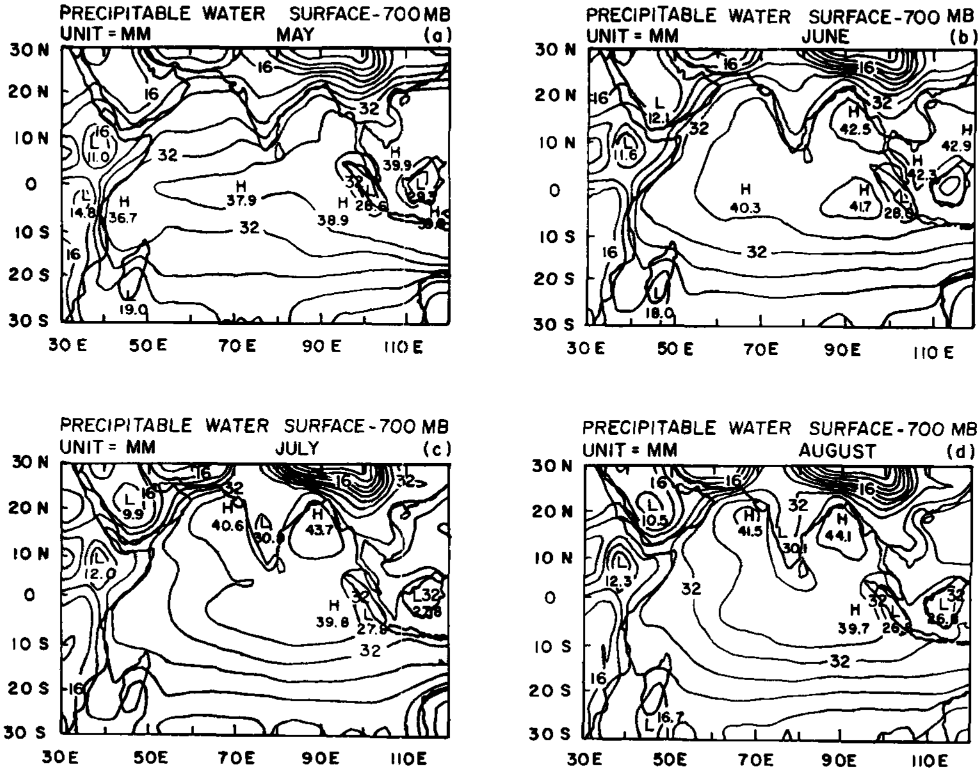

Fig. 9. Monthly mean fields of precipitable water in the layer from the surface to 700 mb. Units are mm. Contour interval is 4 mm. (a) May (b) June (c) July and (d) August.

Arabian coast is drier than in May and June when the convective activity was located near the equator. This relative dryness of the air results from the existence near the coast of Africa of a strong inversion layer preventing the development of convective activity. This inversion layer separates moist air from drier air above about 850 mb (Hart et al., 1978). As our first layer extends from the surface to 700 mb, the drier air above 850 mb gives this feature along the coast of Africa. It does not appear in June because during the first half of the month, preonset conditions prevailed. The inversion becomes weaker eastward and some convection can develop in the eastern Arabian Sea. The increase of PW while the air moves eastward also stresses the importance of evaporation over the Arabian Sea. July 1979 was characterized by a break in the activity of the monsoon. This break does not appear on the monthly mean fields: PW in August (Fig. 9d) is very similar to the July field. This is due to the fact that the break was followed by a revival of the monsoon. The mean field over a month smoothes out such shorter time scale events. During the first 15 days of September (not shown) the intensity of PW over the Arabian Sea decreased but remained high over the Bay of Bengal and over the equatorial area from 75° E to 100° E. The four monthly fields in Fig. 9 depict low values of precipitable water over the Arabian peninsula due to high terrain and dry air. Low values are also found over the elevated plateau of Ethiopia, over the Himalaya mountains, over Sumatra and Borneo Islands. For these three east locations the low values are due to the high elevation.

Fig. 10 gives the monthly mean fields of PW in the layer extending from 700 to 500 mb. May (Fig. 10a) is characterized by high values over the equatorial ocean and low values over the Arabian Sea. This dryness results from the southward circulation from the dry continental Asia. By June (Fig. 10b) PW is higher than 8 mm north of 10° S

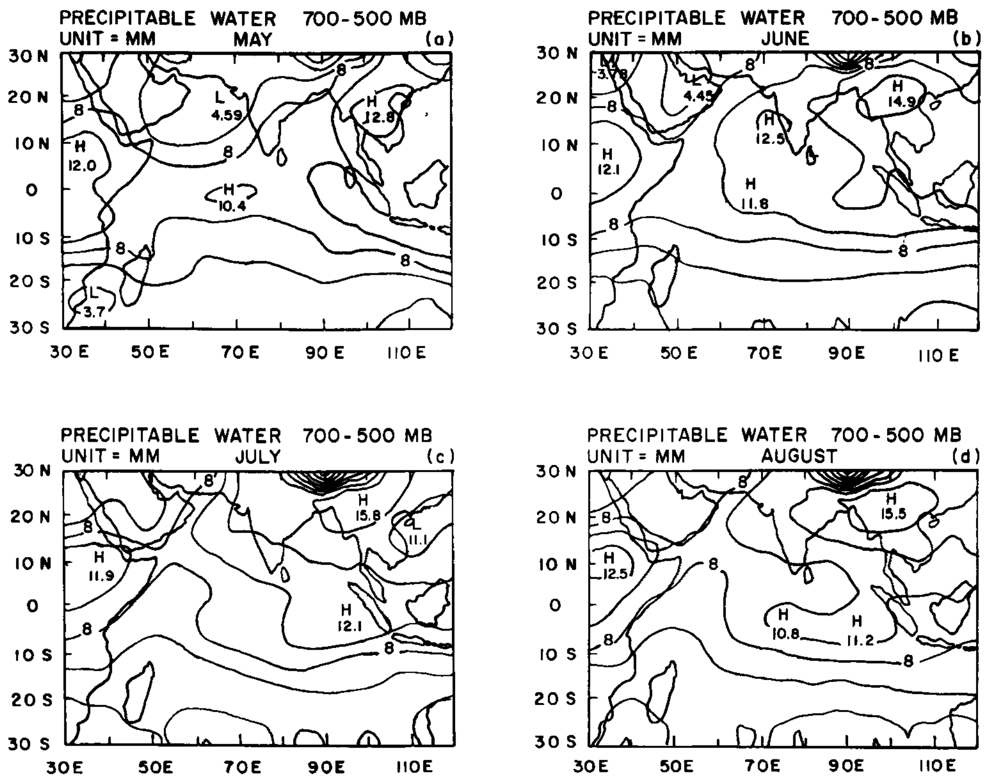

Fig. 10. Same as Fig. 9 except for the layer between 700 and 500 mb. Contour interval is 2 mm.

with the highest values located around India. The high values found off the western coast of India can be associated with the post-onset period when convective activity developed in the eastern part of the Arabian Sea. In July (Fig. 10c) the air is dry from the east coast of Africa up to 60° E due to the existence of the inversion layer. This dryness is more pronounced in the 700–500 mb layer than that in the lowest layer. In August (Fig. 10d), the eastern part of the equatorial Indian Ocean is characterized by large values and the zone of drier air still prevails off the coast of Africa.

Fig. 11 gives the monthly mean fields of PW in the layer extending from 500 to 300 mb. In May (Fig. 11a) the equatorial area and south-east Asia are very humid, whereas all the Arabian Sea north of 10°N is dry. This last feature, as in the fields of the second layer, is due to the northward flow from a dry area typical of pre-monsoon conditions. By June (Fig. 11b) the value of PW over the Arabian Sea has doubled compared to May. The highest values are found around the Indian peninsula whereas the rest of the Arabian Sea is relatively drier. As for the other two layers, this feature can be explained with the existence of a strong inversion layer over the western Arabian Sea becoming weaker and even disappearing in its eastern part. In July (Fig. 11c) the Arabian Sea is drier than in June and a tongue of dry air is extending northward off the coast of Africa: the 2 mm contour line has moved northward by about 10 degrees. In August (Fig. 11d), the eastern part of the equatorial Indian Ocean becomes very humid whereas the Arabian Sea becomes drier indicating the end of the monsoon season.

4. Mean fields during special periods

The onset period is one of the most dramatic periods of the Southwest monsoon season with the increase of the wind intensity over the Arabian Sea

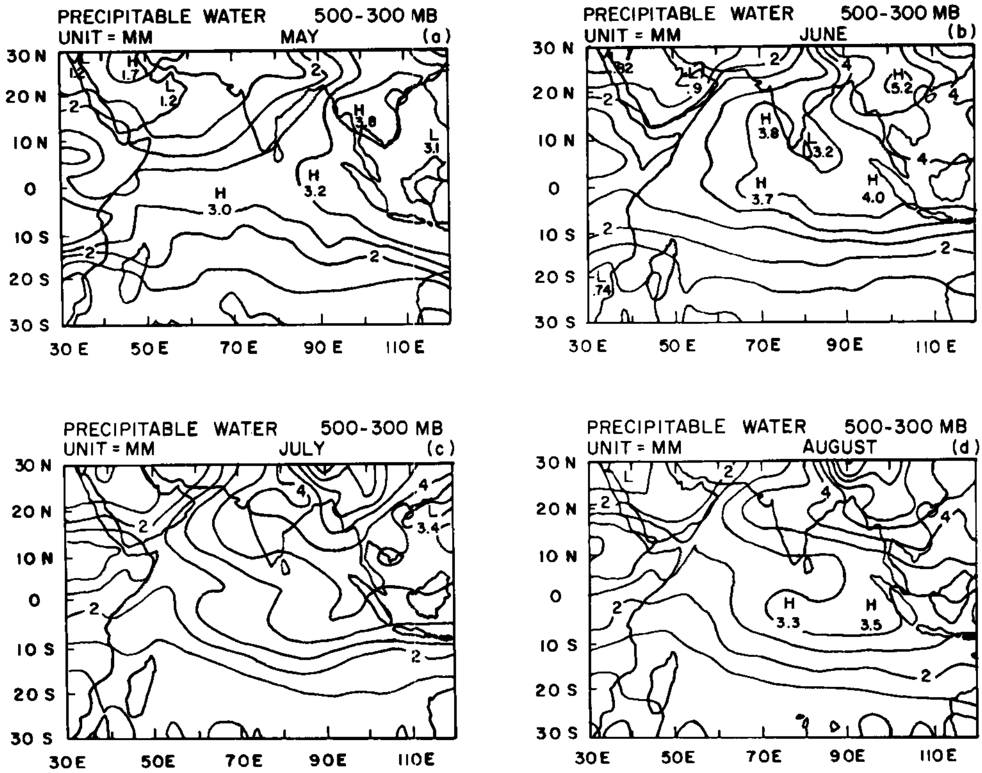

Fig. 11. Same as Fig. 9 except for the layer between 500 and 300 mb. Contour interval is 0.5 mm.

and the first rainfall over the western coast of India. Fig. 12 gives the mean fields of PW for the lower and the upper layers during the first and the second half of June. In the lower layer, high PW over the equatorial Indian Ocean characterized the pre-monsoon conditions. In that layer, starting at the beginning of May, there is a slow increase of the humidity over the Arabian Sea. Thus the 32 mm contour line which was running around 2.5° N during the first half of May reached 7.5° N during the second half of May and moved to 10° N before the onset of the monsoon (Fig. 12a). These conditions are changed with the onset of the monsoon (Fig. 12b). Humidity is higher over India over the Bay of Bengal and over all the Arabian Sea. The formation of an onset vortex (Krishnamurti et al., 1981) on 15 June 1979 can partially explain the large values found off the western coast of India and over northern Arabian Sea also due to convection occurring over the eastern Arabian Sea after the onset. The change of conditions is more drastic in the upper layer where the value of PW doubled within 15 days (Fig. 12c and d). It is particularly interesting to follow the 2 mm contour line. Between the first and second period of May this contour line moved northward of about 5° N and continued to move during the first half of June by 3–4 degrees. During the last weeks of June this contour is located over land. The large value of PW off the western coast of India is due to convection mainly associated during that period with the onset vortex. It is also interesting to note that the Bay of Bengal does not show any increase of PW. In fact, over that area the increase occurred around mid-May. It can also be noted that the amount of PW in the southern part of the domain does not change very much during the periods presented here.

One of the most important characteristics of the monsoon after the onset is its pulsating activity. Rainfall over India which is an indicator of monsoon has two basic synoptic patterns: the

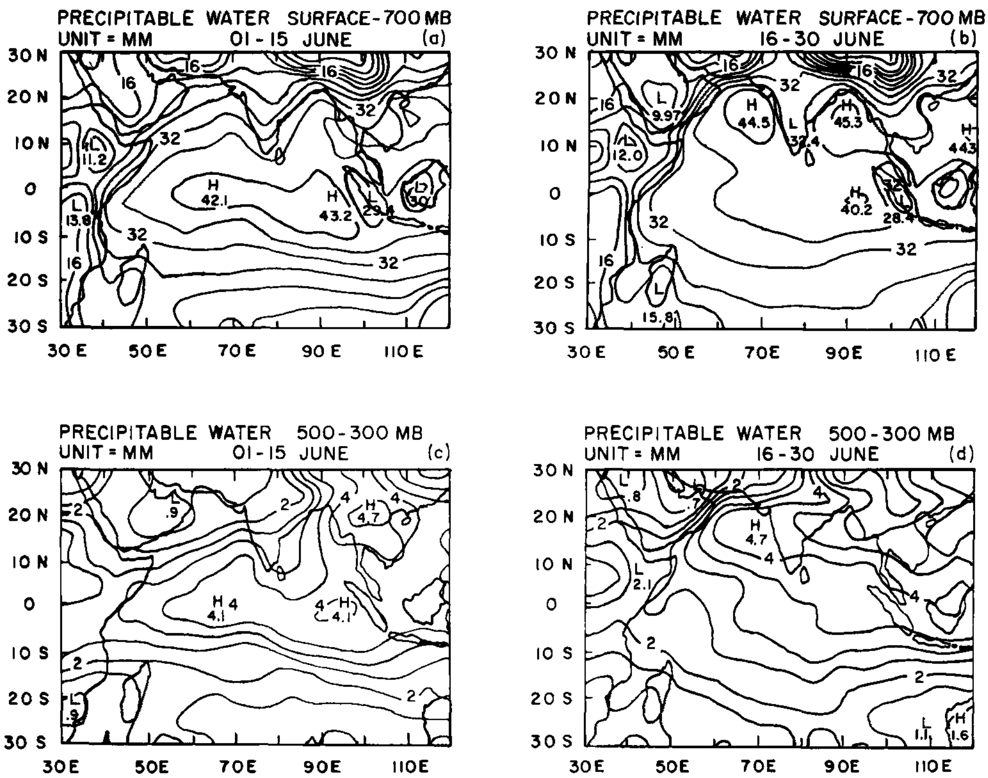

Fig. 12. Mean fields before and after the onset of the monsoon. (a) 1–15 June surface–700 mb contour interval is 4 mm. (b) Same as "a" except 16–30 June. (c) 1–15 June 500–300 mb. Contour interval is 0.5 mm. (d) Same as "c" except 16–30 June.

active and the break (weak) monsoons. The typical time scale lies between 30 and 50 days depending on the year. During the 1979 monsoon only one major break occurred around mid-July. Mean fields of PW in the three layers were determined during active and weak monsoons. The 1979 monsoon was weak over most parts of the peninsula from 11 to 15 July and a break occurred from 16 to 23 July. Two active periods were selected: 14–28 June and 25 July–6 August and the break period from 7 to 18 July. The first active period follows the onset of the monsoon and the second one corresponds to the revival of the monsoon after the break. The selected break period is a few days ahead of the large break period over Central India. The analysis of daily fluctuations of the PW fields over the Arabian Sea shows that PW was minimum between 7 and 18 July, i.e. a few days before the major break over Central India. For the active period, instead of displaying the period just after the onset, we are presenting the revival period after the break.

Fig. 13 gives the PW fields in the upper and lower layers. The difference between the active and weak periods appears mainly over the Arabian Sea. For the lower layer the difference is about 15%. In that layer, the 10 degrees band off the African coast also appears to be drier during weak monsoon. The difference between the two phases of the monsoon are more striking in the upper layer. The 3 mm contour line runs across the Arabian Sea in Fig. 13c whereas it runs along 8° N in Fig. 3d. A tongue of dry air also extends along the African coast. The Bay of Bengal is also drier in the upper layer during the break than during the revival of the monsoon whereas no major change appears in the lowest layer between the two periods.

This decrease of PW in the upper layer related to

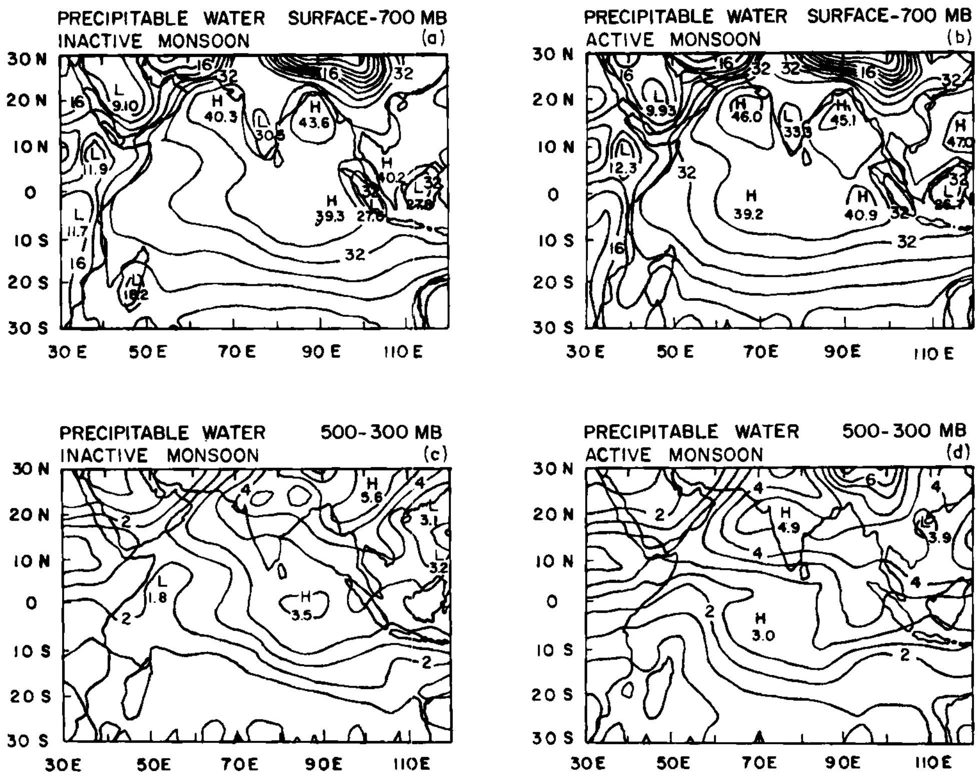

Fig. 13. Mean fields during a break and during a revival period on the monsoon. (a) Surface–700 mb PW fields. 7–18 July. (b) Same as "a" but 25 July–6 August. (c) Same as "a" but PW in the layer from 500 to 300 mb. (d) Same as "b" but PW in the layer from 500 to 300 mb.

the weakening of the activity of the monsoon over India is mainly due to the inhibition of convection over the eastern part of the Arabian Sea. The vertical velocity fields were computed from a vertical integration of the divergence equation assuming a zero vertical velocity at 100 mb. The fields of vertical motion at 500 mb is given in Fig. 14 during the inactive and active monsoons. The active period is characterized by upward motions over a large part of the Arabian Sea indicating convective activity.The break period is characterized by downward motion over the Arabian Sea; the upward motion is only located over the Indian peninsula. Thus, the break corresponds to a decrease of the convective activity, reducing the vertical input of moisture into the mid and upper troposphere explaining the decrease of PW in the upper layer.

5. Time–latitude cross-sections of weekly mean fields

Weekly mean fields were constructed and the time–latitude variations of PW at different longitudes (average over a 10-degree strip) were plotted to show the evolution of the fields at shorter time scales than a month. Time–latitude cross-sections at 60° E and 90° E are discussed.

At 60° E in the first layer (Fig. 15a), PW started to increase near the equator at the beginning of June, i.e. about 2 weeks before the onset of the monsoon. Then, the area of maximum humidity moved northward and reached about 18° N just after the onset of the monsoon. The increase of PW over the Arabian Sea during June is also due to the northward motion of the zone of maximum cloudiness associated with the zone of con-

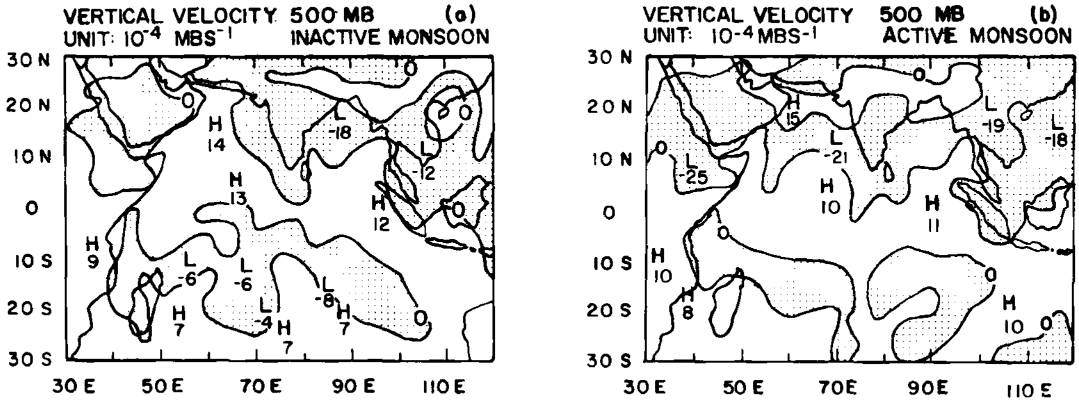

Fig. 14. Field of vertical velocity (10^{-4} mb s^{-1}) at 500 mb over the Indian Ocean during an inactive monsoon (a) and an active monsoon (b). Shaded areas indicate upward motion.

vergence. This slow evolution of the humidity fields before the onset seems to be different from that of the dynamical parameters which change abruptly at the time of the onset. The break in the activity of the monsoon appears during July where low values of PW are found from the equator up to 20° N. This break is followed by a revival period during which PW reached values higher than after the onset of the monsoon.

Fig. 15b depicts the time evolution of the weekly mean value of PW at 60° E in the layer extending from 700 to 500 mb as a function of latitude. The onset period is well-marked with large values appearing near the equator at the end of May and then moving northward to reach 20° N after mid-June. Dry air prevails over the northern part of the Arabian Sea during May: the value of PW tripled between pre and post onset conditions. Starting at the end of June, there is decrease of PW from the equatorial region up to 15° N suggesting a northward propagation of the anomaly. Around 20° N this dry spell is followed by an increase at the beginning of August when the activity of the monsoon resumed. Compared to regions north of the equator, the equatorial area is drier in July and August and becomes more humid by September when the monsoon begins to withdraw from India.

Fig. 15c giving the evolution of PW in the third layer at 60° E is very similar to Fig. 15a and 15b. It shows the northward motion of the zone of maximum humidity during the onset of the monsoon. Dry air prevailed over the equator after the onset phase.

Fig. 16a presents the weekly mean values of PW as a function of latitude at 90° E in the lowest layer. High values of PW are found around 10° N, i.e. in the Bay of Bengal, during all summer whereas low values are prevailing in the equatorial zone. In the middle layer (Fig. 16b) the highest values are located around 10° N before the onset and around 20° N after the onset. The break in the activity of the monsoon can be noted with the northward intrusion of dry air up to 15° N around mid-July. It can be noted that the period of dry air does not appear in the lowest layer (Fig. 16a). In the upper layer (Fig. 16c) May is characterized by low values in the equatorial zone and higher values north of 10° N over the Bay of Bengal. The onset of the southwest monsoon can be noticed when all the area north of 10° S becomes more humid. The highest values are found around 24° N at the end of June. The break in the activity of the monsoon around mid-July is characterized by a reduction of about 50% of PW around 15° N. Thereafter the activity resumes and high values of PW are again found over northern India.

6. Conclusions

Humidity data from the TIROS-N satellite have been analyzed to study the evolution of humidity over the Indian Ocean during the 1979 summer monsoon. TIROS-N precipitable water in three layers has been objectively analyzed with the addition of bogus data in cloudy areas to overcome the inability of the satellite to provide with humidity soundings in such areas. These fields have

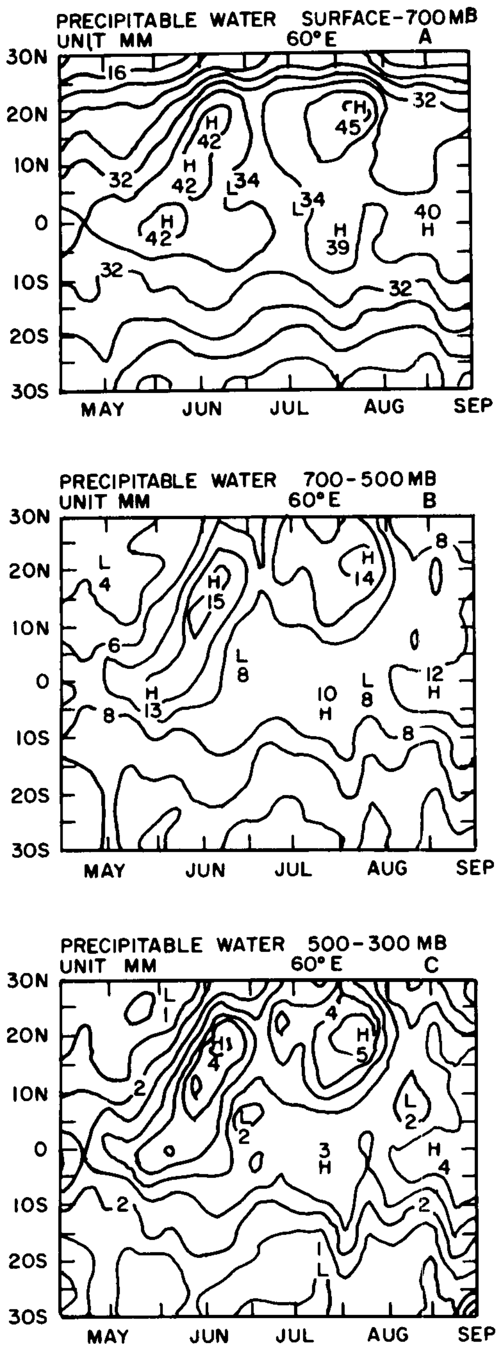

Fig. 15. Weekly mean Precipitable Water as a function of latitude at 60° E. There is an average over a 10° longitude strip. Unit is mm. (a) Layer surface–700 mb. Contour interval is 4 mm. (b) Layer 700–500 mb. Contour interval is 2 mm. (c) Layer 500–300 mb. Contour interval is 0.5 mm.

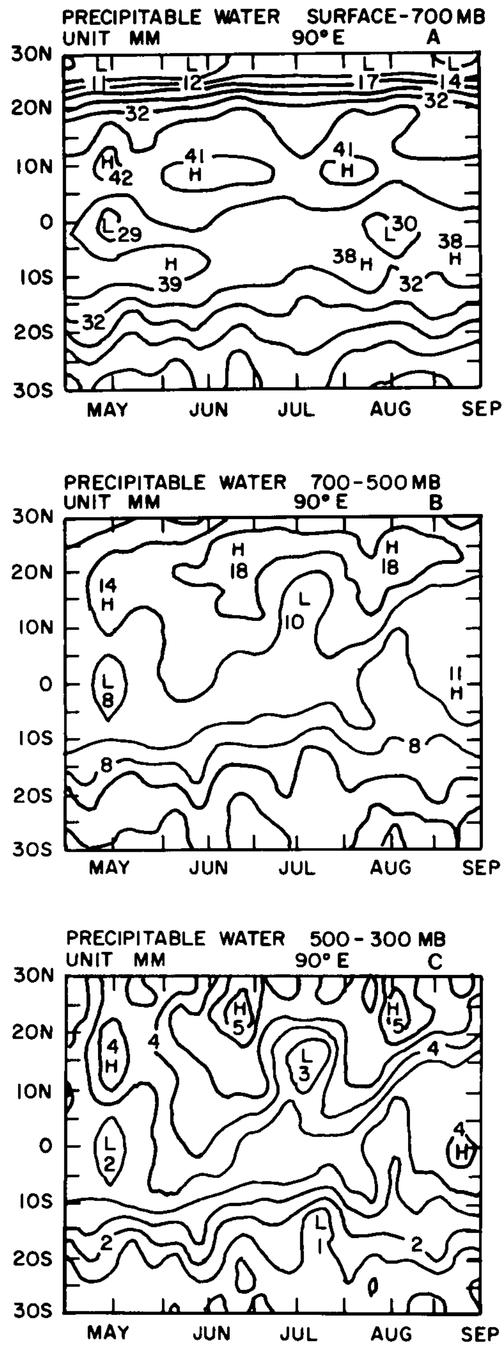

Fig. 16. Same as Fig. 15 except for 90° E.

been merged with fields of PW obtained from the Level III-b data set. The final product compares well with dropsonde soundings performed over the ocean with a relative difference of about 10%.

Different phenomena associated with the summer monsoon give a strong signature on the humidity fields. Thus, the phases of the 1979 monsoon are characterized by large variations of those fields. The features on the PW fields have been described as well as their evolution during the 1979 summer. The build up of moisture associated with the northward progression of the convergence zone before the onset of the monsoon seems to be rather slow compared to the evolution of the dynamical parameters. The thermodynamic structure of the air over the Arabian Sea appears well in the PW fields with relatively dry air along the coast of Africa and more humid air over the western Arabian Sea. The break in the activity of the monsoon around mid-July influences the fields of PW in the three layers, but the upper layer exhibits the stronger relative variation. This can be explained with the inhibition of convective activity over eastern Arabian Sea during the break period.

The method developed to obtain fields of PW can be used to extend the analysis in other areas of the tropics where the assumption on the profile of relative humidity is valid. This method can also be extended at the other latitudes where the different categories of clouds as seen from satellite images can be determined with an assumed relative humidity profile for each category of cloud.

7. Acknowledgement

This work was supported by the National Science Foundation under Grant Number ATM-8120575. I would like to thank Mr. Sam Houston who helped me to run some of the programs necessary to obtain the results. Thanks are also extended to Mrs. Stetson for typing the manuscript.

REFERENCES

Ananthakrishnan, R., Selvan, M. M. and Chellappa, R. 1965. Seasonal variation of precipitable water vapour in the atmosphere over India. *Indian J. Meteorol. Geophys. 16*, 371–384.

Bengtsson, L., Kanamitsu, M., Kållberg, P. and Uppala, S. 1982. FGGE 4-dimensional data assimilation at ECMWF. *Bull. Amer. Meteorol. Soc. 63*, 29–43.

Bergthorsson, R. and Döös, B. 1955. Numerical weather map analysis. *Tellus 7*, 329–340.

Bolhofer, W., Chambers, M., Frey, D., Kuettner, J. and Unninayar, S. 1981. Summer MONEX US Research flight missions, May–July 1979. *NCAR Technical Note*. NCAR/TN–168 + STR.

Cadet, D. 1983. The monsoon over the Indian Ocean during summer 1975. Part II: Break and Active monsoons. *Mon. Wea. Rev. 111*, 95–108.

Cadet, D. and Reverdin, G. 1981a. The monsoon over the Indian Ocean during summer 1975. Part I: Mean fields. *Mon. Wea. Rev. 109*, 148–158.

Cadet, D. and Reverdin, G. 1981b. Water vapour transport over the Indian Ocean during summer 1975. *Tellus 33*, 476–487.

Cressman, G. P. 1959. On operational objective analysis system. *Mon. Wea. Rev. 87*, 367–374.

Gruber, A. and Watkins, C. D. 1979. Preliminary evaluation of initial atmospheric moisture from the TIROS-N sounding system. In: *Satellite Hydrology*, pp. 115–123. M. Deutich, D. R. Wiesnet and A. Rango, eds. Fifth Annual Symposium of the American Water Resources Association.

Gruber, A. and Watkins, C. D. 1982. Statistical assessment of the quality of TIROS-N and NOAA-6 satellite soundings. *Mon. Wea. Rev. 110*, 867–876.

Gupta, M. G. 1981. Intercomparison of data from different observing platforms. Proceeding of the International Conference on the scientific results of the monsoon experiment. Denpasar, Indonesia. Published by WMO, Geneva, Switzerland, pp. 8.20–8.25.

Hayashi, Y. 1980. A method of estimating space-time spectra from polar-orbiting satellite data. *J. Atmos. Sci. 37*, 1385–1392.

Krishnamurti, T. N., Ardanuy, P., Ramanathan, Y. and Pasch, R. 1981. On the onset vortex of the summer monsoon. *Mon. Wea. Rev. 109*, 344–363.

Pathak, P. N. 1982. Comparison of sea-surface temperature observations from TIROS-N and ships in the North Indian Ocean during MONEX (May–July, 1979). *Remote Sensing of Environ. 12*, 363–369.

Ramage, C. S., Miller, F. R. and Jefferies, C. 1972. Meteorological Atlas of the IIOE. Vol. 1: The surface climate of 1963 and 1964. Nation Science Foundation, 144 pp.

Saha, K. R. 1970. Air and water vapour transport across the equator in western Indian Ocean during northern summer. *Tellus 22*, 681–687.

Saha, K. R. and Bavadekar, S. N. 1973. Water vapour budget and precipitation over the Arabian Sea during the northern summer. *Q. J. R. Meteorol. Soc. 99*, 273–278.

Smigielski, F. J. and Mace, L. M. 1970. Estimating mean relative humidity from the surface to 500 millibars by use of satellite pictures. *ESSA*. NESCTM 23. 12pp.

Smith, W. L., Woolf, H. M., Hayden, C. M., Wark, D. Q. and McMillin, L. M. 1979. The TIROS-N operational vertical sounder. *Bull. Amer. Meteorol. Soc. 60*, 1177–1187.

Thompson, A. H. and West, P. W. 1967. Use of satellite cloud pictures to estimate average relative humidity below 500 mb, with application to the Gulf of Mexico area. *Mon. Wea. Rev. 95*, 791–798.

Tripoli, G. J. and Krishnamurti, T. N. 1975. Low-level flows over the GATE area during summer 1972. *Mon. Wea. Rev. 103*, 197–216.